Spanwise Propagation of Upstream Influence in Conical Swept Shock/Boundary-Layer Interactions

G. R. Inger*
Iowa State University, Ames, Iowa

It is shown that the motion within any boundary layer underlying an exactly conical inviscid flow with a swept shock cannot be conical at an arbitrary radial distance r from the origin, and that the resulting viscous-inviscid interaction from the displacement effect of this layer would violate the inviscid conicity. However, the far-field behavior at large radial distances beyond a certain inception length is shown to approach a quasi-two-dimensional state in conical arc length coordinates, a state compatible with the corresponding far-field conical behavior of the overlying inviscid flow including viscous-inviscid interaction effects. Based on an analysis of the governing flow equations for large r, we establish that this inception length is proportional to the product of the interaction zone width (normal to the shock line) and the tangent of the shock sweep angle. These conclusions apply to a wide range of attached shock inviscid flow conditions and boundary-layer states independently of the turbulence modeling, heat transfer, or separation.

Nomenclature

Cp	= constant pressure specific heat, $=\gamma R/(\gamma-1)$
H	= total (stagnation) enthalpy
h	= static enthalpy
h_s	= step height (Fig. 5b)
M	= Mach number
p	= static pressure
R	= gas constant
r,θ,ϕ	= spherical coordinates (Fig. 3)
T	= static temperature
V_r, V_θ, V_ϕ	= velocity components in r,θ, and ϕ directions, respectively (Fig. 3)
x,y,z	= Cartesian coordinates
α	= half-angle of conical shock generator (Fig. 1)
α_{DETACH}	= value of α for shock detachment
γ	= specific heat ratio
δ	= boundary-layer thickness
δ^*	= component displacement thickness
Δ	= three-dimensional thickness, Eq. (15)
ϵ_T	= turbulent eddy viscosity function
λ	$= [(d\delta_o/dX)/(\delta_o/X)]$
Λ	= sweep angle of shock
μ	= coefficient of viscosity
ρ	= density
ℓ_N	= interaction zone width scale normal to shock line
ℓ_θ, ℓ_ϕ	= arc length variables in spherical coordinates (Fig. 4)
ℓ_{INCEP}	= radial inception distance to the onset of conical flow behavior

Subscripts

e	= conditions at boundary-layer edge
o	= undisturbed boundary-layer property
w	= conditions at floor surface
∞	= freestream

Received Nov. 21, 1985; revision submitted June 2, 1986.

*Glenn Murphy Professor, Department of Aerospace Engineering. Associate Fellow AIAA.

I. Introduction

THE question of the spanwise propagation of inboard corner boundary conditions is an important basic question in the design, interpretation, and correlation of experiments on swept shock/boundary-layer interactions.[1] In particular, it is vital to understand the far-field behavior approached by such flows at large outboard distances and to establish the distance required to reach this asymptotic state (the so-called "inception" length). The present paper addresses this question theoretically for the class of conical attached shock generator geometries illustrated in Fig. 1, all of which involve a body standing on a floor that contains a boundary-layer flow. We have chosen this family of shapes because of their relatively straightforward conical inviscid flow solutions and because they have been and are under active experimental study by a number of investigators.[1,2,3]

Section II describes the detailed assumptions and general problem formulation in an appropriate conical coordinate system, followed by an examination of the far-field behavior at large r in both the conical inviscid flow region and the underlying floor boundary layer, including interaction between the two. Section III present an analysis of the approach to this asymptotic behavior that yields a relationship for the inception length. Experimental comparisons supporting this result are also given. Finally, in Sec. IV we summarize our findings and discuss their implications for distinguishing between conically symmetric interactions where properties are constant along radii and cylindrically symmetric interactions where properties are constant along lines parallel to the shock (see Fig. 2).

II. Flowfield Analysis

A. Assumptions

In considering the flow associated with the shock generator geometries of Fig. 1, we restrict attention to attached shock situations where the body deflection angle α is below the detachment value, i.e., the shock is conical and attached. However, the size of α is not otherwise restricted; small disturbances need not be assumed. It is convenient to adopt a spherical coordinate system oriented to the undisturbed shock envelope intercept line in the floor as shown in Fig. 3, since the purely inviscid disturbance field is exactly conical in such a system. The flow is assumed to be the steady motion of a compressible ideal gas of specific heat ratio γ past a floor shock generator geometry that is im-

permeable. Regarding viscous effects, it is further assumed that the Reynolds number based on the incoming boundary-layer thickness is sufficiently large that most of the disturbance region off the face of the shock generator and above the floor is comprised of adiabatic inviscid flow underlaid by a thin, possibly nonadiabatic boundary layer along the body floor. This boundary layer may be either laminar or fully turbulent but not transitional; otherwise, it may be quite general in that interaction with the inviscid flow and perhaps even separation is allowed.

To reveal the essential physical features of the problem without undue complication, we take advantage of this high Reynolds number assumption (which in fact exists in most experimental studies) by retaining only the leading shear stress and heat conduction terms ($\sim \partial^2/\partial y^2$) of classical boundary-layer theory, i.e., we eschew a fully Navier-Stokes formulation. Furthermore, we will not specify any detailed eddy-viscosity modeling scheme in the turbulent case, but assume only that whatever values it provides in the region outboard of the shock generator do not explictly depend on r alone but on the vertical distance y above the floor [which for a thin boundary layer is virtually the same as the spherical arc length ℓ_θ (see Fig. 4)]. Neither do we find it necessary to treat the triple-deck substructure within the viscous-inviscid interaction. Although some of these neglected details can be quantitatively significant in strongly interactive separating flows (e.g., the $\partial p/\partial y$ effect), preliminary analysis including them has shown that they do not alter the essential qualitative results of interest.

B. Inviscid Flow Behavior

Under the assumed neglect of viscous effects or in the inviscid region above the thin floor boundary layer away from the shock generator face, the nature of the physical boundary conditions in Fig. 1 with their lack of any inherent physical scale dictates that the inviscid disturbance flow for an attached shock must be rigorously conical with zero radial gradients in all physical properties. Such a flow would be governed by the following equations in the spherical coordinate notation of Fig. 2:

$$2\rho V_r \sin\theta + \frac{\partial}{\partial\theta}(\rho V_\theta \sin\theta) + \frac{\partial}{\partial\phi}(\rho V_\phi) = 0 \tag{1}$$

$$V_\theta \sin\theta \frac{\partial V_r}{\partial\theta} + V_\phi \frac{\partial V_r}{\partial\phi} - \sin\theta(V_\theta^2 + V_\phi^2) = 0 \tag{2}$$

$$V_\theta \sin\theta \frac{\partial V_\theta}{\partial\theta} + V_\phi \frac{\partial V_\theta}{\partial\phi} + \sin\theta V_r V_\theta - \cos\theta V_\phi^2 + \rho^{-1} \sin\theta \frac{\partial p}{\partial\theta} = 0 \tag{3}$$

$$V_\theta \sin\theta \frac{\partial V_\phi}{\partial\theta} + V_\phi \frac{\partial V_\phi}{\partial\phi} + \sin\theta V_r V_\phi + \cos\theta V_\theta V_\phi + \rho^{-1} \frac{\partial p}{\partial\phi} = 0 \tag{4}$$

$$\left(\frac{2\gamma}{\gamma-1}\right)\frac{p}{\rho} + V_\theta^2 + V_\phi^2 + V_r^2 = \text{const} = 2H \tag{5}$$

which comprise the conservation of mass, of r, θ, and ϕ momentum, and of energy, respectively. In the absence of any three-dimensional interactive effects from the displacement surface of the underlying floor boundary layer, these equations describe the inviscid disturbance flow behavior at all radial distances outboard of the shock generator body. Indeed, a noninteracting analysis of this boundary layer could be carried out along classical lines, if desired, using as input the inviscid pressure gradient and "slip" velocity values of V_ϕ and V_r given by the solution to Eqs. (1-5) with $V_\theta \to 0$ as $\theta \to 0$ (but as will be shown, the resulting boundary-layer flow would, in general, *not* be conical).

We now note an interesting and important property of these conical inviscid flows: their far-field behavior at large values of r (how large this must be will be specified later). This can be seen by dividing Eqs. (1-4) by r and rewriting them in terms of the appropriate spherical arc length coordinates ℓ_θ, ℓ_ϕ defined by $\partial\ell_\theta = r\partial\theta$, $\partial\ell_\phi = r\sin\theta\partial\phi$, respectively (see Fig. 4) to obtain

$$\frac{\partial(\rho V_\theta)}{\partial\ell_\theta} + \frac{\rho V_\theta \cot\theta}{r} + \frac{\partial(\rho V_\phi)}{\partial\ell_\phi} + \frac{2\rho V_r}{r} = 0 \tag{6}$$

$$V_\theta\left(\frac{\partial V_r}{\partial\ell_\theta} - \frac{V_\theta}{r}\right) + V_\phi\left(\frac{\partial V_r}{\partial\ell_\phi} - \frac{V_\phi}{r}\right) = 0 \tag{7}$$

$$V_\theta\left(\frac{\partial V_\theta}{\partial\ell_\theta} + \frac{V_r}{r}\right) + V_\phi\left(\frac{\partial V_\theta}{\partial\ell_\phi} - \frac{V_\phi \cot\theta}{r}\right) + \rho^{-1}\frac{\partial p}{\partial\ell_\theta} = 0 \tag{8}$$

$$V_\theta\left(\frac{\partial V_\phi}{\partial\ell_\theta} + \frac{V_\phi \cot\theta}{r}\right) + V_\phi\left(\frac{\partial V_\phi}{\partial\ell_\phi} + \frac{V_r}{r}\right) + \rho^{-1}\frac{\partial p}{\partial\ell_\phi} = 0 \tag{9}$$

It is immediately seen from these equations that when r is large enough to permit neglect of the various $1/r$ terms compared to the others, the resulting flow is governed by a "quasi-two-dimensional" set of equations in the ℓ_θ, ℓ_ϕ coordinate system. In other words, the far field of the conical disturbance flow asymptotically approaches a Cartesian-like behavior in conical arc length variables ℓ_θ, ℓ_ϕ.

C. Floor Boundary-Layer Behavior in General

Consider next the behavior of the floor boundary layer that would underlie an inviscid conical flow, and how they would interact. Neglecting $\partial p/\partial\theta$ across this thin layer in the leading high Reynolds number approximation and taking $\partial p/\partial r = 0$ from the overlying inviscid flow, either laminar or turbulent nonadiabatic motion is governed by the following equations in the present spherical coordinate system:

$$2\rho V_r \sin\theta + \frac{\partial}{\partial\theta}(\rho V_\theta \sin\theta) + \frac{\partial}{\partial\phi}(\rho V_\phi) = -\sin\theta r \frac{\partial}{\partial r}(\rho V_r) \tag{10}$$

$$\rho\left[V_\theta \frac{\partial V_r}{\partial\theta}\sin\theta + V_\phi \frac{\partial V_r}{\partial\phi} - \sin\theta(V_\theta^2 + V_\phi^2)\right] = -\rho r \sin\theta V_r \frac{\partial V_r}{\partial r} + \frac{\sin\theta}{r}\left\{\frac{\partial}{\partial\theta}\left[(\mu + \rho\epsilon_{T_{r\theta}})\left(\frac{\partial V_r}{\partial\theta} - V_\theta\right)\right] + \cot\theta(\mu + \rho\epsilon_{T_{r\theta}})\left(\frac{\partial V_r}{\partial\theta} - V_\theta\right)\right\} \tag{11}$$

$$\rho\left[V_\theta \frac{\partial V_\theta}{\partial\theta}\sin\theta + V_\phi \frac{\partial V_\phi}{\partial\phi} + \sin\theta V_r V_\phi + \cos\theta V_\theta V_\phi\right] + \frac{\partial p}{\partial\phi} = -\rho r \sin\theta V_r \frac{\partial V_\phi}{\partial r} + \frac{\sin\theta}{r} \times \left\{\frac{\partial}{\partial\theta}\left[(\mu + \rho\epsilon_{T_{\phi\theta}})\left(\frac{\partial V_\phi}{\partial\theta} - V_\phi \cot\theta\right)\right] + 2\cot\theta(\mu + \rho\epsilon_{T_{\phi\theta}})\left(\frac{\partial V_\phi}{\partial\theta} - V_\phi \cot\theta\right)\right\} \tag{12}$$

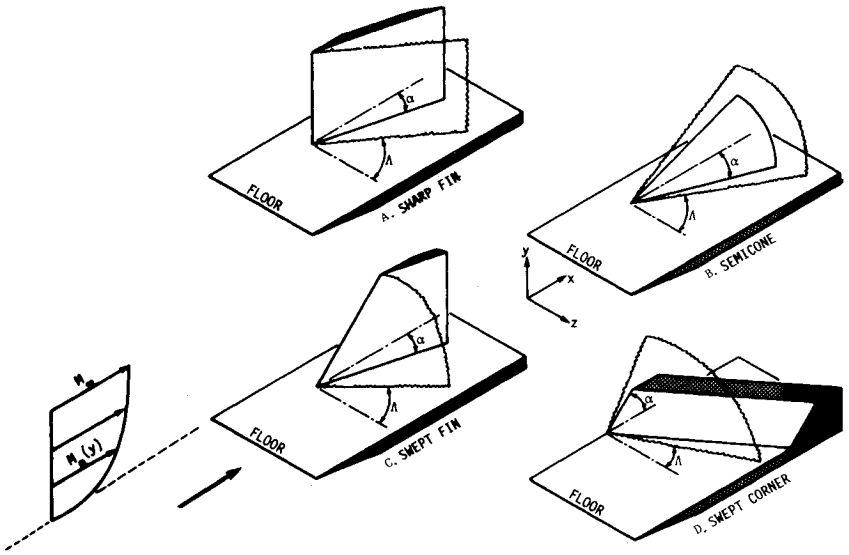

Fig. 1 Examples of conical disturbance flow generators (after Settles and Kimmet[2]).

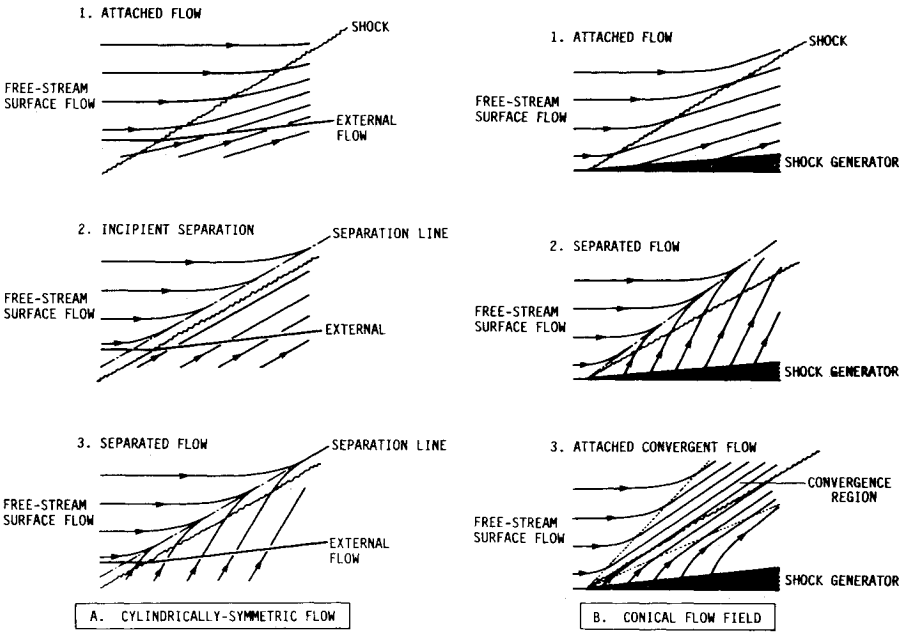

Fig. 2 Typical flow patterns for conical vs cylindrically symmetric interactions (after Kubota and Stollery[11]).

$$\rho\left[V_\theta\frac{\partial h}{\partial\theta}\sin\theta+V_\phi\frac{\partial h}{\partial\phi}\right]+V_\phi\frac{\partial p}{\partial\phi}=-\rho V_r\sin\theta\frac{\partial h}{\partial r}$$
$$+\frac{\sin\theta}{r}\left\{\frac{\partial}{\partial\theta}\left[\left(\frac{\lambda+\lambda_T}{Cp}\right)\frac{\partial h}{\partial\theta}\right]+(\mu+\rho\epsilon_{T_{r\theta}})\left(\frac{\partial V_r}{\partial\theta}\right)^2\right.$$
$$\left.+(\mu+\rho\epsilon_{T_{\phi\theta}})\left(\frac{\partial V_\phi}{\partial\theta}\right)^2\right\} \tag{13}$$

$$\rho h=\gamma p/(\gamma-1) \tag{14}$$

where λ_T is the turbulent eddy conductivity coefficient, the static enthalpy $h=C_pT=\gamma RT/(\gamma-1)$, and where all the terms on the right-hand sides are nonconical effects that explicitly involve either radial gradients or r itself. The accompanying boundary conditions on the solution to these equations along the impermeable floor of some given wall temperature T_w are the no slip conditions $V_\phi(\phi,r,\theta=0)=V_r(\phi,r,o)=0$ and $h(\phi,r,o)=C_pT_w$ with $V_\theta\to 0$, while approaching the outer edge $\delta(\phi,r)$ of the boundary layer we have the inviscid matching conditions $V_\phi(\phi,r,\theta)=V_{\phi e}(\phi,\theta)$, $V_r(\phi,r,\theta)=V_{re}(\phi,\theta)$, $h(\phi,r,\theta)=h_e(\phi,\theta)$ where the e-subscripted values here denote the conical inviscid flow values approaching the surface $\theta\to 0$. [Since $y=r\sin\theta\cos\phi$ (Fig. 3), the small y pertaining to the thin boundary layer on the floor at all (ϕ,r) must imply small θ as well.] The formulation is completed by the expression for the three-dimensional thickness surface $\Delta(r,\phi)$ associated with the mass flow defect of this boundary-layer region:

$$\frac{\partial}{\partial\ell_\phi}[\rho_eV_{\theta e}(\Delta-\delta_\phi^*)]=-\frac{\partial}{\partial r}[\rho_eV_{re}(\Delta-\delta_r^*)] \tag{15a}$$

where

$$\delta_r^*\equiv\int_o^{\delta(r,\phi)}\left(1-\frac{\rho V_r}{\rho_eV_{re}}\right)d\ell_\theta \tag{15b}$$

$$\delta_\phi^*\equiv\int_o^{\delta(r,\phi)}\left(1-\frac{\rho V_\phi}{\rho_eV_{\phi e}}\right)d\ell_\theta \tag{15c}$$

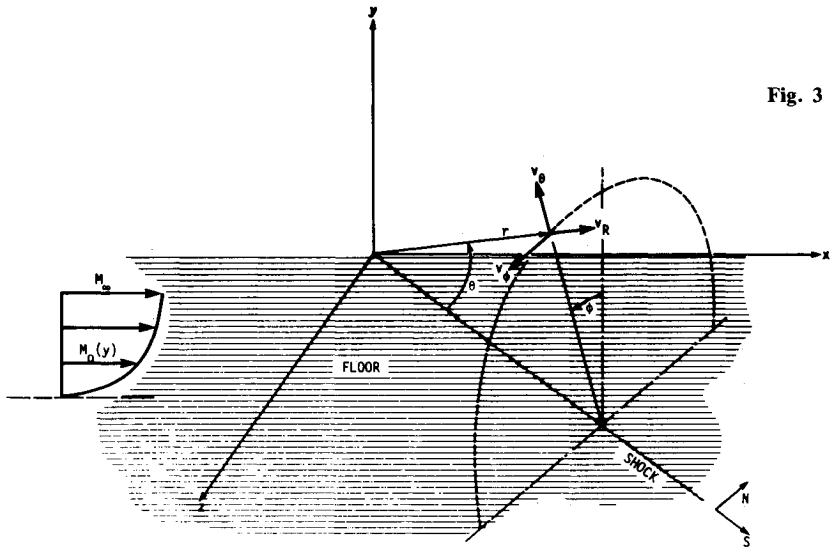

Fig. 3 The shock line oriented spherical coordinate system.

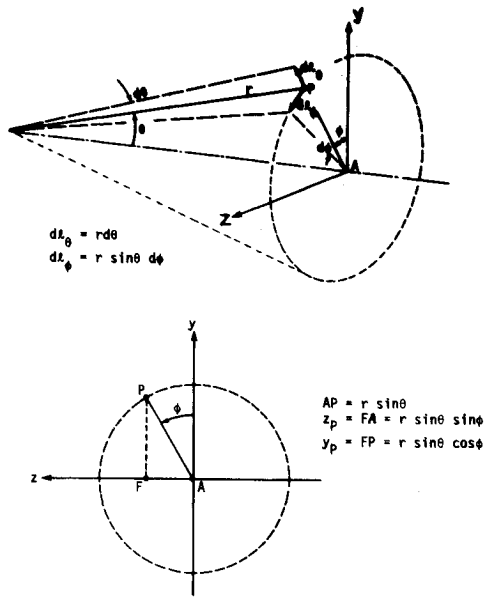

Fig. 4 Arc length and related geometries.

Now it can be readily seen from Eqs. (10–14) and their associated boundary conditions that even in the presence of an exactly conical overlying inviscid flow, the shear stress and heat conduction terms in the θ, ϕ conical variables (whether laminar or turbulent) generally depend on r and hence violate any assumption of conical flow behavior within the boundary layer. Furthermore, the solution of the attendant momentum and energy equations will necessarily yield r-dependent density, V_θ, and V_ϕ profiles which by continuity yield an r-dependent V_r profile as well; all these then require consideration of additional nonconical terms in Eqs. (11) and (12). Thus, the assumption of conical flow behavior is fundamentally incompatible in general with the underlying boundary-layer region, independently of the details of the turbulent eddy viscosity scheme.

A further ramification of this result is evident when we consider the viscous-inviscid interaction that would result from the displacement thickness of the boundary layer. Thus, one sees from Eqs. (15) that the resulting effective floor shape $\Delta(r,\phi)$ seen by the inviscid flow is r-dependent and hence imposes a nonconical distortion of the flow: the interaction effect violates the conicity of an otherwise rigorously conical inviscid flow. [Note that this effect could be alleviated by the use of a suitable nonconical suction distribution that just counterbalances the nonconical contributions to $\Delta(r,\phi)$.]

D. Far-Field Boundary-Layer Behavior

In view of what was shown in Sec. II B, we may ask whether the boundary layer, although inherently nonconical in general, might not have an asymptotic far-field behavior at large r of the same type that was observed for the inviscid flow. The answer is revealed by introducing $\partial\ell_\theta = r\partial\theta$, $\partial\ell_\phi = r\sin\theta\partial\phi$ as before, and rewriting Eqs. (10–13) in arc variable form as follows:

$$\frac{\partial}{\partial\theta_\theta}(\rho V_\theta)+\frac{\rho V_\theta\cot\theta}{r}+\frac{\partial(\rho V_\phi)}{\partial\ell_\phi}+\frac{2\rho V_r}{r}=-\left[\frac{\partial(\rho V_r)}{\partial r}\right] \tag{16}$$

$$\rho V_\theta\left[\frac{\partial V_r}{\partial\ell_\theta}-\frac{V_\theta}{r}\right]+\rho V_\phi\left[\frac{\partial V_r}{\partial\ell_\phi}-\frac{V_\phi}{r}\right]+\left[\rho V_r\frac{\partial V_r}{\partial r}\right]$$
$$=\left\{\frac{\partial}{\partial\ell_\theta}\left[(\mu+\rho\epsilon_{T_{r\theta}})\left(\frac{\partial V_r}{\partial\ell_\theta}-\frac{U_\theta}{r}\right)\right]\right.$$
$$\left.+\frac{\cot\theta}{r}\left(\frac{\partial V_r}{\partial\ell_\theta}-\frac{U_\theta}{r}\right)(\mu+\rho\epsilon_{T_{r\theta}})\right\} \tag{17}$$

$$\rho V_\theta\left[\frac{\partial V_\phi}{\partial\ell_\theta}+\frac{V_\phi\cot\theta}{r}\right]+\rho V_\phi\left[\frac{\partial V_\phi}{\partial\ell_\phi}+\frac{V_r}{r}\right]+\frac{\partial p}{\partial\ell_\phi}$$
$$+\left[\rho V_r\frac{\partial V_\phi}{\partial r}\right]=\left\{\frac{\partial}{\partial\ell_\theta}\left[(\mu+\rho\epsilon_{T_{\phi\theta}})\left(\frac{\partial V_\phi}{\partial\ell_\theta}-\frac{V_\phi\cot\theta}{r}\right)\right]\right.$$
$$\left.+2\frac{\cot\theta}{r}\left(\frac{\partial V_\phi}{\partial\ell_\theta}-\frac{V_\phi\cot\theta}{r}\right)(\mu+\rho\epsilon_{T_{\phi\theta}})\right\} \tag{18}$$

$$\rho\left(V_\theta\frac{\partial h}{\partial\ell_\theta}+V_\phi\frac{\partial h}{\partial\ell_\phi}\right)+V_\phi\frac{\partial p}{\partial\ell_\phi}=\frac{\partial}{\partial\ell_\theta}\left[\left(\frac{\lambda+\lambda_T}{Cp}\right)\frac{\partial h}{\partial\ell_\theta}\right]$$
$$-\left[\rho V_r\frac{\partial h}{\partial r}\right]+(\mu+\rho\epsilon_{T_{r\theta}})\left(\frac{\partial V_r}{\partial\ell_\theta}\right)^2$$
$$+(\mu+\rho\epsilon_{T_{\phi\theta}})\left(\frac{\partial V_\phi}{\partial\ell_\theta}\right)^2 \tag{19}$$

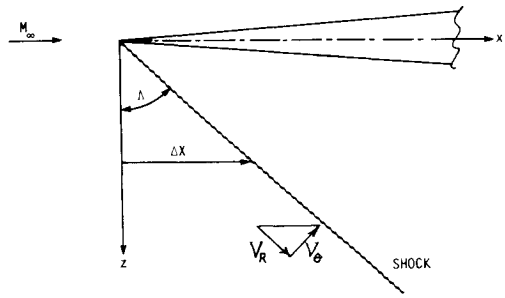

Fig. 5 Incoming boundary-layer property variation due to shock sweep.

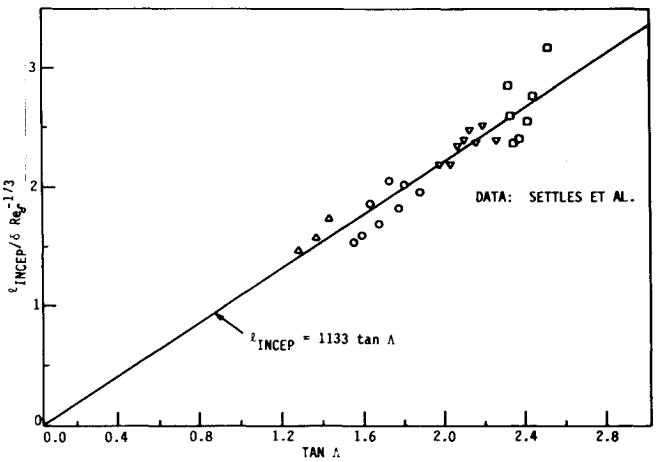

Fig. 6 Experimental data on inception length vs shock sweep angle for fin-induced turbulent interactions.

Now under the assumption that $\epsilon_{T\theta}$, $\epsilon_{T\phi\theta}$, and λ_T each depend only on ℓ_θ and ℓ_ϕ, these equations indicate that where the various terms $\sim 1/r$ are neglected for large r (see below for further discussion), there indeed does exist a meaningful quasi-two-dimensional boundary-layer problem in ℓ_θ, ℓ_ϕ that is otherwise independent of r (the residual radial derivative terms now being permissibly dropped, indicated by boldface brackets). Moreover, this asymptotic behavior is completely compatible with the overlying conical inviscid flow including viscous-inviscid interaction effects as well: under the stated asymptotic conditions, Eqs. (15) reduce to

$$\frac{\partial}{\partial \ell_\phi}[\rho_e V_{\phi e}(\Delta - \delta_\phi)] \to 0 \tag{20a}$$

or

$$\Delta(r,\phi) \to \delta_\phi \tag{20b}$$

so that the resulting quasi-two-dimensional displacement effect on the overlying inviscid flow is still compatible with its far-field conical nature. We re-emphasize that this important result is quite general, having been obtained independently of the details of the heat transfer, turbulence modeling (this model may in fact be nonisotropic since $\epsilon_{T\theta}$ and $\epsilon_{T\phi\theta}$ are here allowed to be inequal), any triple-deck structure of the viscous-inviscid interaction zone, or any separation that might be present.

At this point, we address an effect that might violate this far-field quasi-two-dimensional behavior: the streamwise variation $\delta_o(X)$ of the incoming undisturbed boundary-layer thickness (on which the interaction depends) in the presence of a swept shock (see Fig. 5). Writing this variation as

$$\delta_o(X) \cong \delta_o(X_o) + \left(\frac{d\delta_o}{dX}\right)_{X_o} \cdot \Delta X$$

and noting that $d\delta_o/dx \approx \lambda\delta_o/X$ for laminar ($\lambda = 1/2$) or turbulent flow ($\lambda \simeq 1/5$), respectively, we have upon expressing $\Delta X = r\sin\Lambda$ that

$$\delta_o(X) = \delta_o(X_o)\left(1 + \lambda\frac{r}{X_o}\sin\Lambda\right)$$

Now it is seen that the second term in parenthesis, which represents an explicitly nonconical effect $\sim r$, is in fact negligible whenever the local value of $\lambda r \sin\Lambda$ is much smaller than the upstream boundary-layer development distance X_o. If $X_o \gg \lambda r$, as is often true in regions of experimental observation, the questioned effect is insignificant even for large sweep angles. A similar argument can be made regarding the undisturbed shape factor and skin friction variations along ΔX (which also can affect the interaction), leading to the same conclusion.

III. The Inception Distance

A. Order-of-Magnitude Analysis

Having established the character of the far-field flow, we now proceed to examine in detail the conditions under which it is valid. Among other things, this will lead to an expression for the inception distance $r > \ell_{INCEP}$ beyond which the entire interactive flowfield is essentially quasi-two-dimensional in the conical arc length variables ℓ_θ, ℓ_ϕ.

Inspection of Eqs. (16–19) shows that the various $1/r$ terms (and hence $\partial/\partial r$ effects) may be rigorously neglected if the following inequalities are satisfied:

Continuity and ϕ momentum:

$$V_r/r \ll V_\phi/\ell_\phi \tag{21}$$

$$V_\theta \lesssim V_r \tan\theta \tag{22}$$

r momentum:

$$V_\phi/r \ll V_r/\ell_\phi \tag{23}$$

$$V_\phi \lesssim V_\theta \tag{24}$$

θ momentum (inviscid):

$$V_r/r \ll V_\theta/\ell_\theta \tag{25}$$

$$V_\phi^2(\cot\theta/r) \lesssim V_r V_\theta/r \tag{26}$$

We note in this regard that

$$V_\phi/\ell_\phi \sim V_\theta/\ell_\theta \tag{27}$$

in order that all the retained terms are of the same order; also note that the energy equation adds nothing more. Deferring momentarily an examination of the first two conditions and taking the others in turn, we find by substituting $\ell_\phi = (r\sin\theta)\,\phi = FA = \phi/\sin\phi$ (Fig. 4) into Eq. (23) that it requires

$$|FA|/r \ll (\sin\phi/\phi)(V_r/V_\phi) \tag{28}$$

Now $\sin\phi/\phi$ and V_r/V_ϕ are both generally of order unity, while FA in the region close to the floor is a measure of the interactive width scale ℓ_N normal to the shock line (Fig. 4); therefore, Eq. (28) requires physically that ℓ_N must be small compared with r, a condition that is usually met in the outboard region of the flows illustrated in Fig. 1, except perhaps when there is massively extensive separation. Proceeding to Eq. (24) we see that it merely embodies the nonrestrictive general requirement that V_ϕ and V_θ be of the same order. By virtue of Eq. (27), Eq. (25) is equivalent to Eq. (21), while Eq. (26) reduces to the statement that

$V_\phi \lesssim (V_\theta/V_\phi) \times V_r \tan\theta$ which in view of Eq. (24) becomes the same thing as Eq. (22). Therefore, provided Eq. (28) is satisfied, Eqs. (21) and (22) are sufficient to insure the desired quasi-two-dimensional far-field behavior.

Equation (22) infers that the upwash velocity approaching the floor ($\theta \to 0$) must become very small compared to the radial velocity, which is indeed true at any r for all high Reynolds number interactions. Moreover, this condition is also satisfied in the vicinity of the shock line $\theta = 90 - \Lambda$ where $V_r/V_\theta = \cot\theta$. Turning to Eq. (21), then, we see that it serves to delimit how large r must be for the flow to attain the desired asymptotic behavior. Again using Eq. (27) plus the expression for ℓ_ϕ and noting Eq. (24), it can be rewritten as

$$r > |FA|\,(V_r/V_\theta) \tag{29}$$

When applied to the interaction region near the floor where $|FA| \sim \ell_N$ and $V_r/V_\theta \sim \tan\Lambda$ (Fig. 5), we thus get the statement that $r > \ell_{INCEP}$ where ℓ_{INCEP} is the desired radial inception length of order

$$\ell_{INCEP} \sim C\ell_N \tan\Lambda \tag{30}$$

Here, C is an unknown constant of order unity that depends on the details of the inboard nonconical interactive boundary-layer flow (which are beyond the scope of the present paper); in general, it would depend on the Reynolds and Mach numbers, on the incoming boundary-layer shape factor and the wall temperature, and strongly on the specific shock generator shape.[9] Otherwise, the result [Eq. (30)] applies to all conical interactions in stating that the inception distance scales directly with the product of the tangent of the shock sweep angle and the interactive width scale (say the upstream influence distance) normal to the floor shock line. It is noteworthy that Stalker[3] has also given an argument in support of this $\tan\Lambda$ dependence based on consideration of the relative tangential to normal mass-flow ratio of the swept shock.

B. Comparisons with Experiment

Since Λ and ℓ_N are both often known in experiments on swept shock/boundary layer interactions, observations of ℓ_{INCEP} in such tests can be used to check the validity of Eq. (30). (In so doing, one must be careful to exclude a number of experiments wherein the maximum lateral scale is in ℓ_{INCEP} and which are thus dominated throughout by inboard nonconical effects.[4]) It is noted for this purpose that we can alternatively express Eq. (30) as

$$\ell_{INCEP}/\delta_o = C' \tan\Lambda \tag{31}$$

where $C' = C\ell_N/\delta_o$ is a constant large in magnitude compared to unity when $\ell_N/\delta_o \gg 1$.

A comprehensive study of the inception length for many fin-generated conical interactions (Figs. 1a and 1c) has recently been reported by Settles[3]; his correlation of the observed variation of ℓ_{INCEP} with the sweep angles involved at $M_\infty = 2.95$ is reproduced in Fig. 6. It is seen that these data strongly support the present prediction that $\ell_{INCEP} \sim \tan\Lambda$. Moreover, using the nominal mean values $\delta_0 \approx 5$ mm and $Re_\delta \approx 6.4 \times 10^7$/m pertaining to these experiments,[5] Settles' correlation relation shown in Fig. 6 yields $\ell_{INCEP} \approx 16.6 \tan\Lambda$ in qualitative agreement with Eq. (31). Also, Eq. (31) agrees with his conclusion that the "inception zone is... the response of the flow to an input boundary-layer length scale,"[3] which in turn is supported by the fin-interaction experiments of Zubin and Ostapenko[6] who showed that ℓ_{INCEP} becomes vanishingly small when δ_o is reduced to near zero.

Further verification is obtained from some measurements on the spanwise growth of the upstream influence outboard of a Mach 2 fin interaction (Fig. 1a) by Dolling.[7] His results, shown in Fig. 7, indicate that $\ell_{INCEP}/\ell_N \tan\Lambda \approx 1.8$, in qualitative agreement with Eq. (30). This equation also tends to explain the extremely small inception lengths observed in strongly hypersonic swept shock interactions,[8,9] where the corresponding upstream influence distances are found to be very small.

In closing this discussion, we note that the foregoing comparisons pertain to an adiabatic wall condition. Since T_w and

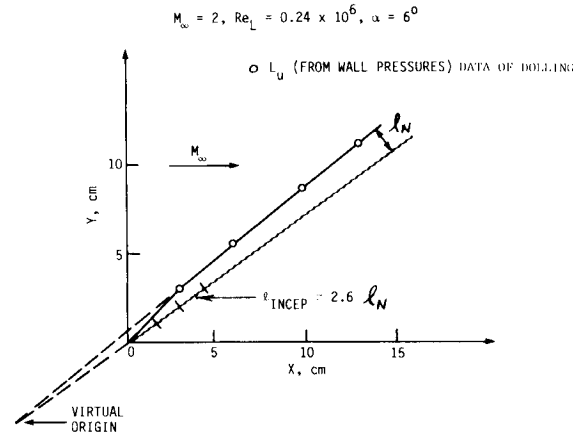

Fig. 7 Data on spanwise growth of upstream influence on a Mach 2 fin/turbulent boundary-layer interaction.

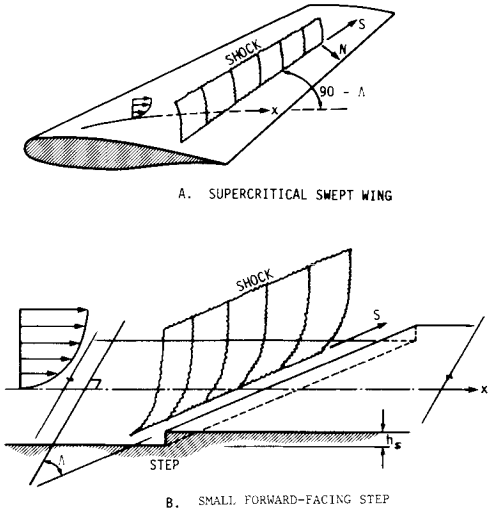

Fig. 8 Some practical examples of cylindrically symmetric interactive flows.

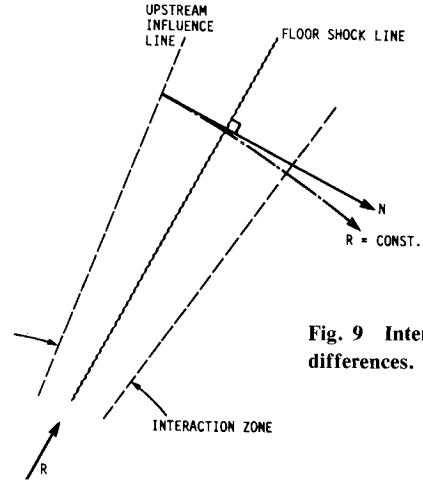

Fig. 9 Interaction zone coordinate differences.

δ_o increase monotonically with M_∞ above $M_\infty \sim 2$–3, this suggests that the ℓ_{INCEP} of an adiabatic flow would also increase with Mach number. On the other hand, if the wall is instead maintained at a highly cooled condition as is frequently the case in hypersonic wind-tunnel tests and in flight, the resulting reduction of δ_o implies from Eq. (31) that ℓ_{INCEP} may be significantly smaller than observed in adiabatic experiments at moderate supersonic Mach numbers.

IV. Concluding Remarks

In summary, we have shown rather generally that the motion within any boundary layer underlying an exactly conical inviscid flow with a swept shock cannot be conical at arbitrary radial distance from the origin, and indeed that the resulting viscous-inviscid interaction from the displacement effect of this layer would violate the inviscid conicity. However, it was shown that the far-field behavior at large radial distances beyond a certain inception length, approaches a quasi-two-dimensional state in conical arc length coordinates that is compatible with the corresponding far-field conical behavior of the overlying inviscid flow including viscous-inviscid interaction effects. Based on an order-of-magnitude analysis of the governing flow equations for large r, we deduced an estimate of this inception length showing it to be proportional to $\ell_N \tan\Lambda$ provided ℓ_N/r is very small. These conclusions apply to a wide range of attached inviscid flow conditions and boundary-layer states independently of the turbulence modeling, heat transfer, separation, etc., and are considered to be all the more useful for this reason.

In conclusion, we will briefly comment on the question of how conically symmetric interactions such as those considered here may be distinguished from those with so-called cylindrical symmetry[10] in the case of attached shock configurations. Two essential features basically differentiate between them: 1) the nature of the global boundary conditions and the resulting inviscid flow solution they yield, and 2) the shape of the surface isobars in the viscous-inviscid interaction region outboard of the inception zone, i.e., whether they are radial or parallel lines (see Fig. 2). Regarding the first, it is clear that if the inboard shock generator shape (including the influence of any vertical planes of symmetry) yields a conical shock envelope *and* contains no inherent length scale, the resulting inviscid solution and outboard far field must be conical with constant properties along radii. On the other hand, if there is no inboard shock generator but a straight swept normal shock such as on a large aspect ratio supercritical wing or a swept surface distortion with a definite scale length such as a small step of small height h_s (see Fig. 8), then the inviscid solution would necessarily follow a cylindrically symmetric pattern. The second feature is self-explanatory and consistent with the first, except to note that in situations where the interaction zone width is a small fraction of the local radius (i.e., a weak turbulent interaction), it may be very difficult in practice to discern the difference between variations along a short radial arc length appropriate to a conical far field and those along the short normal to a straight shock line (see Fig. 9). When this is the case, one must decide on the basis of the first feature, i.e, the character of the inviscid behavior demanded by the global boundary conditions involved.

Acknowledgment

The support of this research by Air Force Office of Scientific Research Grant 85-0357 (Dr. James Wilson, monitor) is gratefully acknowledged, as are stimulating discussions with Professors Gary Settles, Seymour Bogdonoff, and David Dolling.

References

[1]Settles, G. S. and Dolling, D. S., "Swept Shock Wave-Boundary Layer Interactions: A Survey," *Progress in Astronautics and Aeronautics, Tactical Missile Aerodynamics*, edited by M. J. Hemsch and J. N. Nielsen, AIAA, New York, Vol. 104, 1986, pp. 297–379.

[2]Settles, G. S. and Kimmel, R. L., "The Similarity Law of Conical Shock Wave/Turbulent Boundary-Layer Interactions," *AIAA Journal*, Vol. 24, Jan. 1986, pp. 47–53.

[3]Settles, G. S., "On the Inception Lengths of Swept Shock Wave/Turbulent Boundary Layer Interactions," *Proceedings of 1985 IUTAM Symposium on Turbulent Shear Layer/Shock Wave Interactions*, Palaiseau, France, Sept. 1985, pp. 203–214.

[4]McClure, W. B. and Dolling, D. S., "Flow Field Scaling in Sharp Fin-Induced Shock Wave Turbulent Boundary Layer Interaction," AIAA Paper 83-1754, July 1983.

[5]Settles, G. S. and Lu, F. K., "Conical Similarity of Shock/Boundary Layer Interactions Generated by Swept and Unswept Fins," *AIAA Journal*, Vol. 23, July 1985, pp. 1021–1027.

[6]Zubin, M. A. and Ostapenko, N. A., "Structure of Flow in the Separation Region Resulting from Interaction of a Normal Shock Wave with a Boundary Layer in a Corner," *Mekhanika Zhidosti i Gaza 3*, 1979, pp. 51–58.

[7]Dolling, D. S., "Upstream Influence in Sharp Fin-Induced Shock Wave/Turbulent Boundary Layer Interaction," *AIAA Journal*, Vol. 21, Jan. 1983, pp. 143–145.

[8]Holden, M., "Experimental Studies of Quasi-Two-Dimensional and Three-Dimensional Viscous Interaction Regions Induced by Skewed Shock and Swept Shock/Boundary Layer Interactions," AIAA Paper 84-1677, June 1984.

[9]Law, C. H., "Three-Dimensional Shock Wave/Turbulent Boundary Layer Interactions at Mach 6," USAF ARL-TR-75-0191, June 1975.

[10]Settles, G. S. and Teng, H. Y., "Cylindrical and Conical Flow Regimes of Three-Dimensional Shock/Boundary Layer Interactions," *AIAA Journal*, Vol. 22, Feb. 1984, pp. 194–200.

[11]Kubota, H. and Stollery, J. L., "An Experimental Study of the Interaction Between a Glancing Shock Wave and a Turbulent Boundary Layer," *Journal of Fluid Mechanics*, Vol. 116, 1982, pp. 431–458.